scientific reports

Check for updates

OPEN

High-performance spinel $NiMn_2O_4$ supported carbon felt for effective electrochemical conversion of ethylene glycol and hydrogen evolution applications

Shymaa S. Medany[1]✉, Mahmoud A. Hefnawy[1]✉ & Soha M. Kamal[2]

One of the most effective electrocatalysts for electrochemical oxidation reactions is $NiMn_2O_4$ spinel oxide. Here, a 3-D porous substrate with good conductivity called carbon felt (CF) is utilized. The composite of $NiMn_2O_4$-supported carbon felt was prepared using the facile hydrothermal method. The prepared electrode was characterized by various surface and bulk analyses like powder X-ray diffraction, X-ray photon spectroscopy (XPS), Scanning and transmitted electron microscopy, thermal analysis (DTA), energy dispersive X-ray (EDX), and Brunauer–Emmett–Teller (BET). The activity of $NiMn_2O_4$ toward the electrochemical conversion of ethylene glycol at a wide range of concentrations was investigated. The electrode showed a current density of 24 mA cm^{-2} at a potential of 0.5 V (vs. Ag/AgCl). Furthermore, the ability of the electrode toward hydrogen evaluation in an alkaline medium was performed. Thus, the electrode achieved a current density equal 10 mA cm^{-2} at an overpotential of 210 mV (vs. RHE), and the provided Tafel slope was 98 mV dec^{-1}.

The escalating global need for energy has been the catalyst for the advancement of sustainable and environmentally conscious alternative energy sources that have the potential to supplant conventional fossil fuels. The utilization of fossil fuels is linked to various constraints, such as the emission of greenhouse gases and the finite nature of these resources. Researchers have also directed their attention toward other intelligent alternatives[1–4].

Alkaline direct alcohol fuel cells (ADAFCs) powered by compact organic molecules have exhibited potential as portable energy solutions[5,6]. In comparison to traditional low-temperature hydrogen fuel cells, liquid fuel cells have several advantages. Its advantages include increased density and theoretical energy efficiency, enhanced safety measures, and increased transportability and storage convenience. Ethylene glycol (EG) possesses significant promise as a feasible fuel alternative for use in ADAFCs, owing to its enhanced energy density and boiling point compared to methanol and ethanol. Furthermore, empirical evidence suggests that ethylene glycol's oxidation rate is greater in an alkaline medium than in an acidic medium. A wide variety of catalyst materials can be utilized in alkaline settings, demonstrating significant catalytic efficiency while still being reasonably cost-effective. In an alkaline environment, ethylene glycol undergoes complete oxidation, resulting in the liberation of a total of 10 electrons per molecule, as illustrated below[7]:

$$(CH_2OH)_2 + 10OH^- \leftrightarrow 2\,CO_2 + 8\,H_2O + 10e^- \quad (1)$$

Xin et al.[8] recommended two reaction paths for ethylene glycol (EG) conversion in their study. These pathways involve the creation of oxalate via glycolate oxidation and the cleavage of the carbon–carbon (CC) bond in EG, resulting in the reproduction of species and the ultimate formation of carbonate. In contrast to previous research, Miyazaki et al.[9] proposed a unified pathway consisting of a series of chemical steps: EG → glycolate → oxalate → CO_2 → carbonate. The production of glycolate and carbonate appeared to occur via a common intermediate, whereas oxalate appeared to be generated by the oxidation of desorbed glycolate[10,11].

Nevertheless, the successful integration of EG fuel cells into the commercial sector necessitates the availability of anode catalysts for ethylene glycol oxidation reaction (EGOR) that exhibit exceptional efficiency and

[1]Department of Chemistry, Faculty of Science, Cairo University, Giza 12613, Egypt. [2]Applied Electrochemistry Laboratory, Chemistry Department, Faculty of Science, Beni-Suef University, Beni-Suef 52511, Egypt. ✉email: shymaasamir80@cu.edu.eg; shymaa@sci.cu.edu.eg; maadel@cu.edu.eg; maahefnawy@gmail.com

cost-effectiveness. Extensive research has been conducted on EGOR over a considerable period of time, with a specific focus on its conduct on various metal and modified metal electrodes. The electrodes utilized in this study consist of platinum (Pt), palladium (Pd), gold (Au), cobalt (Co), iron (Fe), and nickel (Ni). Previous research on these electrodes has predominantly focused on experiments conducted in alkaline environments[12–18]. Pt and Pt-based catalyst anodes play a crucial role due to their high efficiency towards the electrochemical oxidation of the EG and the ability to facilitate reactions at lower potential values. Nevertheless, it should be noted that the cost of these materials is very high and they are susceptible to contamination by CO-adsorbed species[19,20]. Nickel-based materials have garnered considerable interest in the field of electrocatalysis due to their remarkable catalytic capabilities in facilitating the reactions of diverse small organic molecules. These materials encompass metallic nickel, nickel oxides, hydroxides and oxyhydroxides, as well as nickel alloys and composites. Therefore, these materials have been widely utilized as anodic catalysts for electrooxidation processes in recent decades[21–23].

A technique known as the hydrogen evolution reaction (HER) uses an electric current to turn water into hydrogen gas. Fuel cells, electricity generation, and chemical synthesis are just a few uses for hydrogen, a clean and renewable energy source[24,25]. Hydrogen evolution reactions (HER) play a vital role in reducing The reliance on fossil fuels, which serve as a notable contributor to atmospheric pollution and the release of greenhouse gases. The primary objective of the HER is to address and alleviate the adverse impacts that arise from the extraction and transportation of fossil fuels on both ecosystems and human health. Furthermore, the utilization of high-efficiency rectifiers (HER) facilitates the smooth incorporation of sustainable energy sources, such as solar and wind power, into the preexisting energy framework. Due to their intermittent and variable characteristics, renewable energy sources pose challenges for grid stability and storage.

Carbon felt (CF) as support was used extensively in electrocatalysis field[26–30]. It was an attractive support to the scientists due to its properties for this different metal forms were loaded on its surface. *Pierożyński* et al. prepared ruthenium-modified nickel-coated carbon fiber and studied its performance as an electrocatalyst for hydrogen evolution reaction[26]. Koca et al. modified the carbon felt by NiGa for hydrogen production purposes. The authors proved that the presence of Ga on Ni/carbon felt reduces the hydrogen evolution potential of the electrode and provide higher current passages[27]. Ece Altunbaş Şahin was prepared AgCo/CF, using an electrochemical deposition process, a little amount of Ag was deposited over Co-deposited Carbon felt and examined for HER performances in an alkaline medium[31]. The authors proved that the binary AgCo/CF has a high current density of 159.71, 574.10, and 1640.2 mA.g.C at different potentials obtained from cathodic current potential curves of $i_{-1.2V}$, $i_{-1.3V}$, and $i_{-1.4V}$; respectively[31]. Manganese-based materials have received a great attention from researchers toward HER, and/or OER, i.e. water splitting[32]. Fe doped Ni_3S_2/MnS was found to have a high catalytic activity towards OER[33]. The combination of heterojunction, which enhances the catalyst's conductivity, modifies the active site's electrical configuration, and maximizes the adsorption capacity of intermediates containing oxygen to produce quick reaction kinetics and excellent catalytic performance, is responsible for the increased catalytic activity[33]. Zhu et al. prepared Se-MnS/NiS heterojunctions as highly efficient bifunctional electrocatalysts for overall water splitting[34]. The electrocatalysis of HER and OER may benefit from the addition of the Se dopant, which could modify the structure and raise the electrochemically active surface area. Furthermore, in comparison to the NiSe, NiS, and Se-NiS catalysts, the synergistic impact of the Se-MnS/NiS heterojunctions encouraged the adsorption of hydrogen atoms on the catalyst's surface. The resulting Se-NiS/MnS catalyst was able to provide a 10 mA cm^{-2} current density for HER and OER in alkaline media, respectively, with overpotentials as low as 56 mV and 211 mV. Additionally, Se-MnS/NiS demonstrated exceptional endurance for 48 h and a comparatively low voltage of 1.47 V at 10 mA cm^{-2} when used directly as bifunctional electrodes for total water splitting[34].

For the previous reasons, we aimed in our study to synthesize nickel manganese spinel oxide supported on carbon felt, via the hydrothermal method, as electrocatalyst for EGOR and hydrogen production. In an alkaline medium, the activity of modified NMO-CF for ethylene glycol electrooxidation and hydrogen production was investigated. The surface characterizations of the prepared electrocatalyst were studied using several surface techniques. Different electrochemistry techniques were utilized to determine the activity of the modified electrode.

Experimental section

Preparation of $NiMn_2O_4$-CF (NMO-CF)

All the chemical reagents utilized in this study were of analytical grade and were not subjected to additional processing. The synthetic pathway is depicted in Fig. 1. To improve the wettability of the carbon felt (CF), a treatment was conducted using a mixture of H_2SO_4 and H_2O_2 in a volume ratio 1:3. The treatment duration was 3 h at a temperature of 80 °C. Subsequently, CF was thoroughly rinsed with deionized water. Then, the sample was subjected to sonication in ethanol for 30 min, followed by a drying period of 3 h at a temperature of 80 °C[35,36].

Furthermore, the objective of this procedure was to eliminate the impurities and enhance the surface roughness of carbon fiber filaments. The $NiMn_2O_4$-CF (NMO-CF) composite material was synthesized using a straightforward hydrothermal method. Initially, a total of 2.07 g of cobalt (II) nitrate hexahydrate ($Mn(NO_3)_2.6H_2O$), 1.03 g of nickel(II) nitrate hexahydrate ($Ni(NO_3)_2{\cdot}6H_2O$), and 1.28 g of urea ($CO(NH_2)_2$) were dissolved in 30 mL of deionized water. The resulting mixture was then subjected to stirring for 20 min at a temperature of 60 °C. As a result of this process, a transparent pink solution was formed. Subsequently, the homogeneous precursor solution was carefully transferred into a Teflon-lined stainless-steel autoclave with a volume of 45 mL. The pretreated carbon felt, measuring approximately 1 cm × 1 cm × 2 mm, was immersed in the solution and allowed to remain submerged for 3 h at different temperatures. After cooling to ambient temperature, the acquired specimen was subjected to a thorough rinsing with deionized water and subsequently subjected to a drying period of 3 h at a temperature of 80 °C. Ultimately, the specimens underwent annealing in a nitrogen (N_2) environment at a temperature of 350 °C for 4 h.

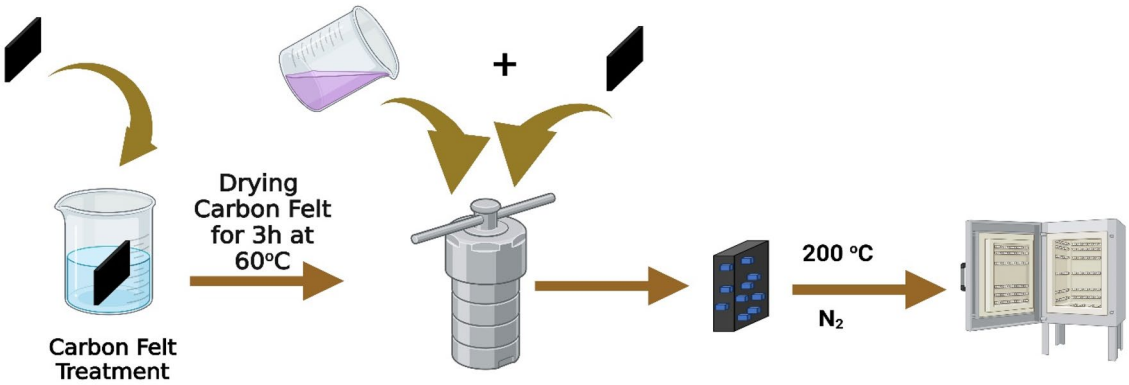

Figure 1. Schematic representation of NMO-CF preparation.

Electrode preparation

The electrochemical studies were utilized upon modified carbon felt with a 1 cm × 1 cm × 2 mm dimension. In order to evaluate the activity of the NMO-CF electrode towards the electrooxidation of ethylene glycol (EG), electrochemical investigations were carried out by cyclic voltammograms, chronoamperometry, and electrochemical impedance spectroscopy. 1.0 M NaOH aqueous electrolyte, a platinum wire as the counter electrode, and an Ag/AgCl (saturated KCl) as the reference electrode were employed in the three-electrode setup to conduct the necessary tests.

To conduct several electrochemical studies, such as cyclic voltammetry, chronoamperometry, and electrochemical impedance, an AUTOLAB workstation (PGSTAT128N) was used. The graphical user interface was created using Nova software (version 2.1). In order to measure the EIS experiment, an AC potential was applied that ranged from 0.1 Hz to 10^4 Hz.

Result and discussion

Analysis

The chemical structure of the prepared spinel oxide and modified carbon felt composite were characterized using several surface and bulk analytical techniques. However, powder X-ray diffraction was employed to confirm the chemical structure of prepared spinel oxides.

Figure 2 depicts the composite $NiMn_2O_4$ spinel oxide. The diffraction peaks observed at angles of 18.6°, 30.15°, 35.71°, 37.34°, 43.6°, 57.07°, 62.78° and 57.8° can be attributed to the diffraction planes (111), (220), (311), (222), (400), (511), (440) and (533) of the spinel $NiMn_2O_4$, as depicted in Fig. 2. The observed peaks strongly correlate with the JCPDS No. 36–0083 and the findings described in the existing literature[37–40].

XPS analysis examined the surface atomic concentration and valence states of $NiMn_2O_4$ composites. Figure 3a displays the high-resolution XPS spectra of $NiMn_2O_4$ composites, which include the typical peaks for Mn (2p), Ni (2p), and O (1s) states. The X-ray photoelectron spectroscopy (XPS) analysis of nickel (Ni) revealed distinct peaks at energy levels of 854.6 eV and 871.7 eV, corresponding to the Ni ($2p_{3/2}$) and Ni ($2p_{1/2}$) electronic states, respectively. The observed discrepancy in binding energy, commonly referred to as spin-energy separation, which amounts to approximately 18 eV, provides evidence of Ni^{2+} ions within the $NiMn_2O_4$ composites[41–45].

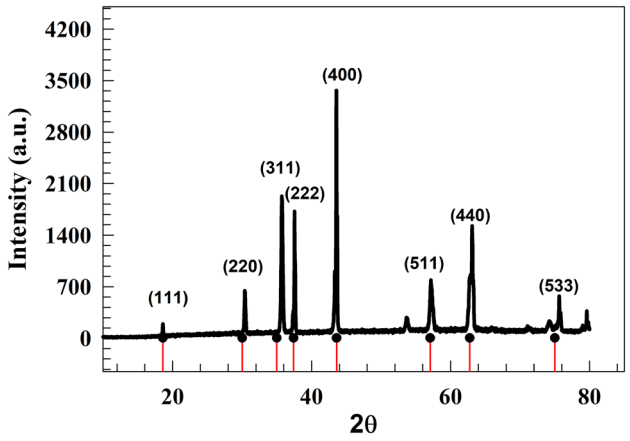

Figure 2. XRD chart of $NiMn_2O_4$.

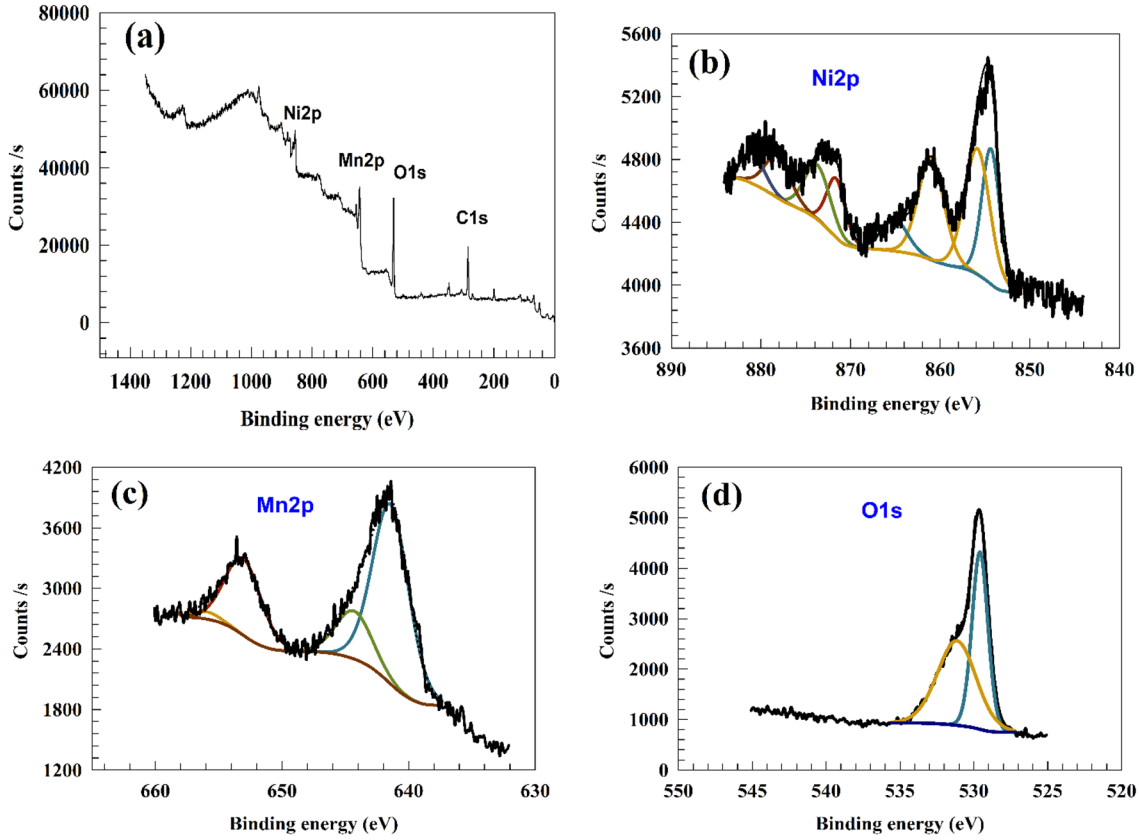

Figure 3. (**a**) survey of $NiMn_2O_4$, (**b**)Ni 2p, (**c**) Mn 2p, (**d**) O1s.

The Ni2p peaks observed at binding energy of 854.6 and 856.46 eV are corresponding to $2p_{3/2}$ Ni^{2+} and Ni^{3+} peaks[46,47]. The peaks seen at around 861.3 and 864.8 eV correspond to the satellite of $Ni2p_{3/2}$. The peaks observed at 871.48, 874.34 eV, 878.6 and 881.03 eV correspond to the $2p_{1/2}$ state and the satellite of the $Ni2p_{1/2}$ state, respectively[48–50]. Two supplementary peaks of shakeup satellites can be observed at energy levels of 860.8 eV and 878.7 eV, as depicted in Figure 3b.

However, the presence of two distinct peaks at 655.3 and 641.7 eV in Figure 3c can be attributed to the $Mn2p_{1/2}$ orbital of Mn^{2+} ions and the $Mn2p_{3/2}$ orbital of Mn^{3+} ions, respectively[51].

The peaks observed at 644.7 and 655.3 eV in the spectrum correspond to Mn^{3+} ions, while the peak at 641.7 eV is attributed to Mn^{2+} ions[52]. The doublet Mn 2p, which exhibits a spin-orbit splitting of approximately 11.6 eV, is attributed to the presence of Mn^{3+}. Figure 3d displays the deconvolution spectra for the O 1s, comprising three components. The lattice oxides (O^{2-}) ions exhibited distinct peaks at 529.6 and 531.1 eV, which are typical of their composition.

The morphology of modified and unmodified were studied using high-resolution scanning electron microscopy (SEM). Figure 4a shows the unmodified carbon fiber felt in the nanoparticles' absence. Whereas the pretreatment of the carbon felt leads to the absence of contamination on an unmodified surface. The uniform distribution of active components on the CF fibers is investigated by examining scanning electron microscopy (SEM). Firstly, according to the data presented in Figure 4b, the surface of CF exhibits a uniform texture characterized by the presence of fine particles of $NiMn_2O_4$. As represented in Figure 4c, higher magnification of modified carbon felt showed a well-distribution of nanoparticles. Thus, nanoparticles with cubic structure shape were observed with a range of 75 ~ 120 nm.

The scanning electron microscopy (SEM) photographs obtained after 5 hours of electrolysis reveal a predominant similarity in the form of the NMO-CF electrode compared to its initial state before the prolonged operation (see Figure 4d). This observation confirms the remarkable stability exhibited by the suggested electrode material.

The use of energy-dispersive X-ray spectroscopy (EDX) is an essential methodology that facilitates the identification of the elemental ingredients of a provided surface. Moreover, it is employed to visually depict the spatial distribution of chemical components across the photographed area. The EDX obtained from the NMO-CF sample depicted in Figure 4e confirmed the presence of nickel (Ni), manganese (Mn), oxygen (O), nitrogen (N), sulfur (S), and carbon (C). Identifying components in the energy-dispersive X-ray (EDX) spectrum indicates the effective synthesis of the nickel manganese spinel oxide with a ratio between Ni and Mn of 1 to 2.

Furthermore, the morphological structure of $NiMn_2O_4$ was characterized by TEM. Figure 5a represents the particle size of 16 ~ 50 nm. Whereas, the cubic structure observed in XRD chart can be localized in TEM image. As represented in Figure 5b, the diffraction of $NiMn_2O_4$ confirm the presence of hkl of (111), (220), (400), and (440). Figure 5c shows lattice spacing of $NiMn_2O_4$ that the measured spacing corresponds to planes of (220), and (111) of $NiMn_2O_4$ crystals.

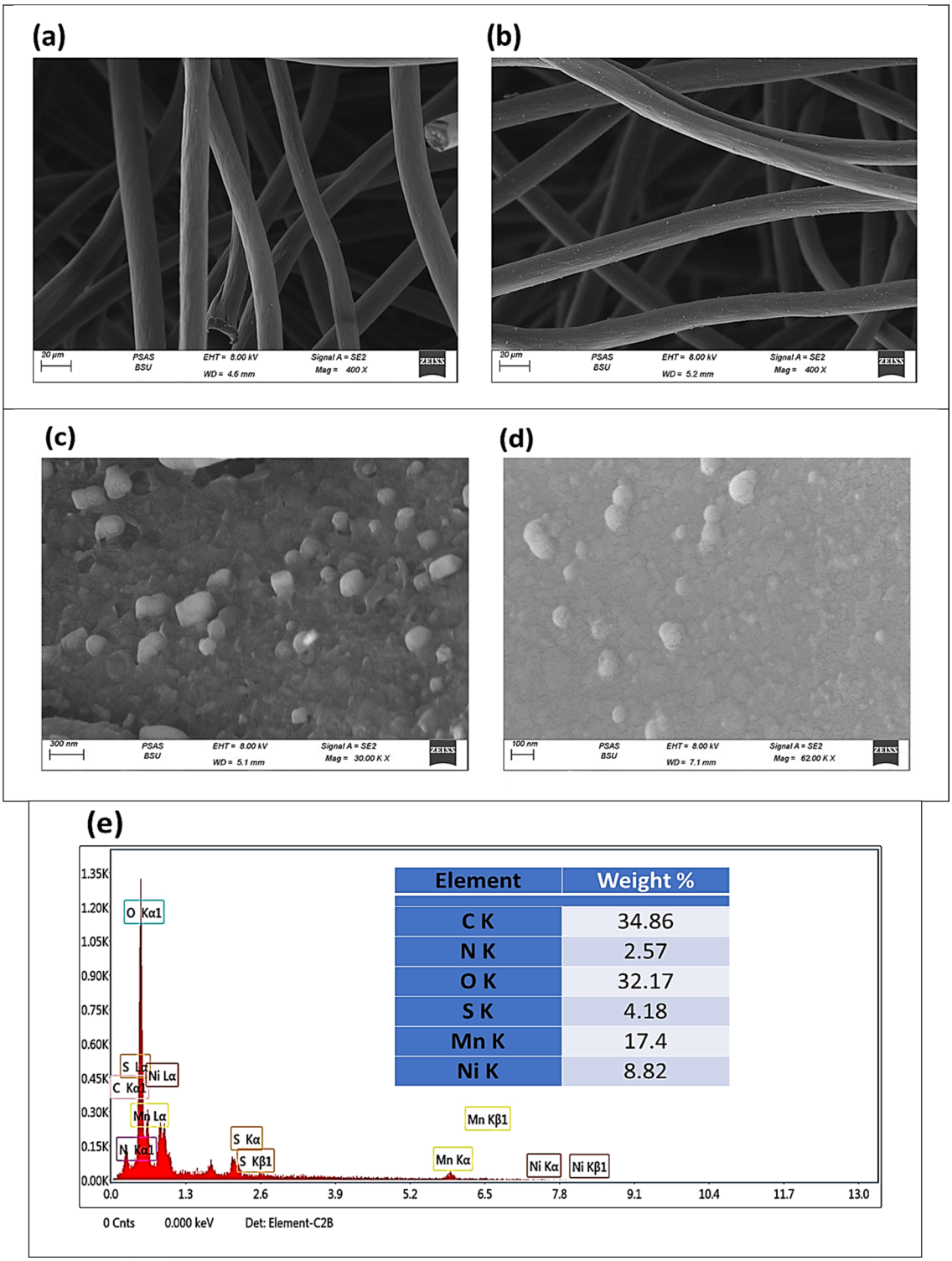

Figure 4. (**a**) Pristine CF, (**b**) NMO-CF, high magnification of NMO-CF, (**c**) before oxidation, (**d**) after oxidation, (**e**) EDX of NMO-CF.

Figure 5d presents the differential thermal analysis (DTA) curves of the NMO-CF. As evident from the DTA curve, the initial breakdown stage commences at 519°C and concludes at 553°C with integration (-0.65 µV) attributed to the breakdown of the carbon felt. The second observed transition at 601 to 628 °C for integration of – 0.188 µV for carbon felt carbonization. The final stage was observed at 659 to 732, corresponding to converting residual oxide to spinel oxide with integration – 0.782 µV.

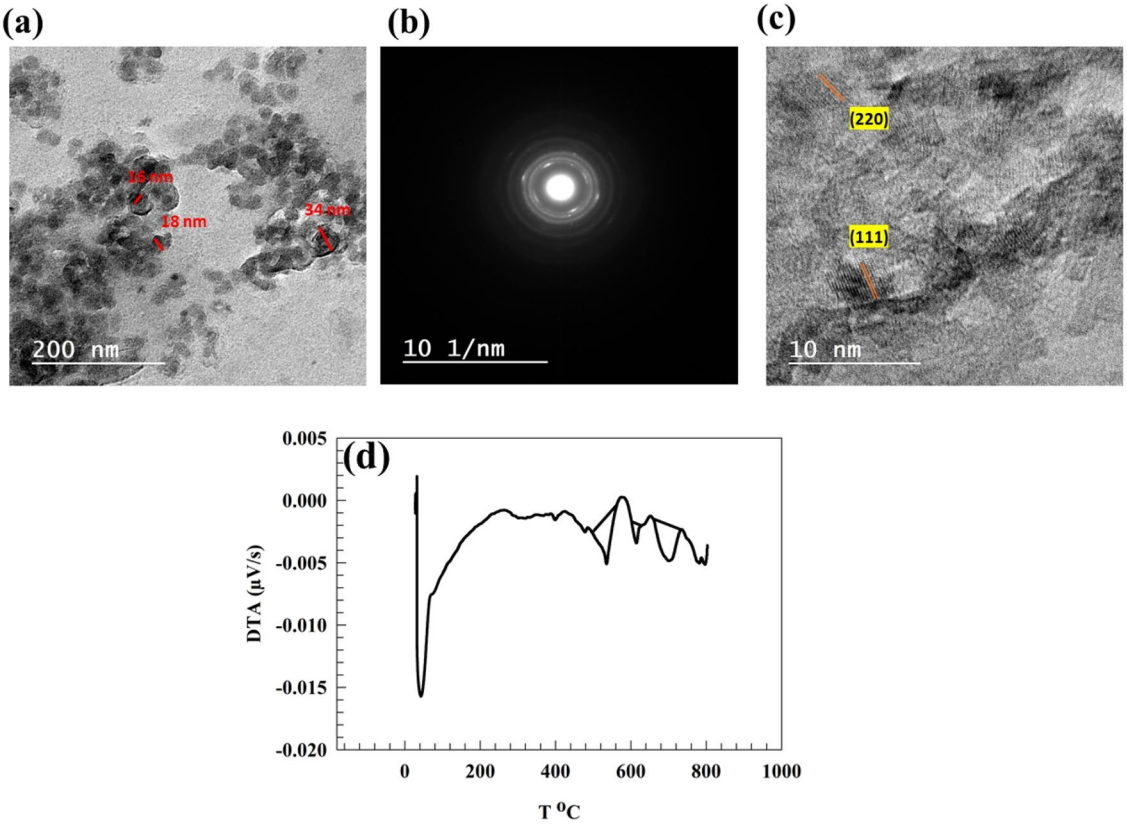

Figure 5. (**a**) TEM of $NiMn_2O_4$, (**b**) diffraction, (**c**) lattice spacing, (**d**) DTA of $NiMn_2O_4$-CF.

The surface and porosity of the pristine carbon felt, and modified NMO-CF were investigated using BET analysis. The analysis was performed by nitrogen adsorption without thermal correction at a pass temperature of 77.4 K and worm-free space of 10.3814 cm^3.

A type III isotherm was observed, typical of microporous materials. Therefore, the BET surface area for unmodified and modified carbon felt was 13.28 and 328.24 m^2/g, respectively. Moreover, the estimated adsorption average pore diameter for pristine CF and NMO-CF were 6.569 and 0.350 nm, respectively.

From BET analysis, our prepared electrocatalyst $NiMn_2O_4$/CF exhibited higher surface area (328.24 m^2/g) over the other $NiMn_2O_4$ present in the literature. The surface area values for CuS/$NiMn_2O_4$ NCs[53], $NiMn_2O_4$/CNF[54], and $NiMn_2O_4$[55], were found to be 54.83, 193, and 59.9 m^2/g.

Electrochemical investigation

Ethylene glycol oxidation

According to the oxidation mechanism of ethylene glycol compounds on Ni-based catalysts, NiOOH plays a catalytic function, and the oxidation steps takes place after $Ni(OH)_2$ is converted to NiOOH[56,57].

As a result, the following is the suggested mechanism on a nickel-based catalyst as follows[58]:

$$Ni(OH)_2 + OH^- \leftrightarrow NiOOH + e^- \tag{2}$$

$$Ni^{2+} + HOCH_2CH_2OH \leftrightarrow Ni^{2+}(HOCH_2CH_2OH)_{ads} \tag{3}$$

$$Ni^{2+}(HOCH_2CH_2OH)_{ads} + 2\,NiOOH \leftrightarrow Ni^{2+}(HOCH_2CHO)_{ads} + 2\,Ni(OH)_2 \tag{4}$$

$$Ni^{2+}(HOCH_2CHO)_{ads} + 2\,NiOOH + OH^- \leftrightarrow Ni^{2+}(HOCH_2COO^-)_{ads} + 2\,Ni(OH)_2 \tag{5}$$

The electrode was first activated in KOH to create metal hydroxides and regenerate active species. The electrode was subjected to 50 cycles in a solution of 1.0 M NaOH at a scan rate of 20 mV s^{-1}.

Figure 6 displays the CVs of ethylene glycol electrochemical oxidation on the surface of NMO-CF in a solution of 1.0 M NaOH and 1.0 M fuels at a scan rate of 20 mV s^{-1}. In the absence of ethylene glycol, only the redox peak observed attributed to the conversion of Ni(II)/Ni(III). Moreover, the addition of ethylene glycol led to the formation of distinctive oxidation peaks corresponding to the oxidation of ethylene glycol.

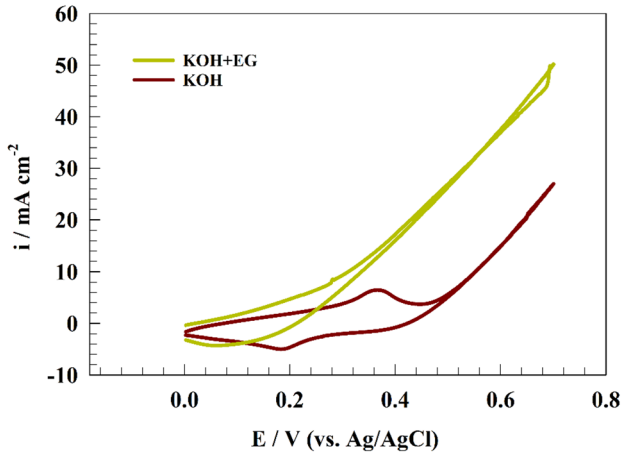

Figure 6. CV of modified NMO-CF electrode in the presence and absence of 1.0 M ethylene glycol.

The carbon felt as a catalyst support has been extensively employed, particularly in cases where the catalyst exhibits restricted ethylene glycol oxidation activity. However, the application of CF has been found to enhance the electrode surface's electrical conductivity and improve the catalyst's stability.

The presence of active NiOOH species primarily influences ethylene glycol conversion. The calculation of surface coverage was performed using Eq. (6) in the absence of ethylene glycol for various scan rates ranging from 5 to 200 mV s^{-1}. The equation provided can be estimated as follows[11]:

$$I_p = \frac{n^2F^2}{4RT}\upsilon\ A\ \Gamma \tag{6}$$

where Ip is current for EG oxidation, n is the number of consumed electrons, F is Faraday constant, A is electrode area, and Γ is surface coverage.

Figure 7a represents the CV of the modified NMO-CF electrode in 1.0 M NaOH in the absence of EG at a wide scan range. The surface coverage was established using a linear relation between oxidation current versus the scan rate (see Fig. 7b). Thus, the surface coverage provided for the modified surface was 7.66×10^{-7} cm s^{-1}.

The investigation also encompassed the examination of the electrochemical reaction exhibited by the NMO-CF modified electrode in response to changes in the fuel concentration. The experiment involved altering the concentration of ethylene glycol within the solution, ranging from 0.05 M to 1.0 M. The solution also contained 1.0 M KOH; the scan rate used was 20 mV s^{-1}, as depicted in Fig. 8a. The observed phenomenon indicates a positive correlation between the concentration of ethylene glycol and the magnitude of the anodic peak current. The data presented in this study suggests that the utilization of the proposed composite material shows promise for ethylene glycol electrooxidation in applications like fuel cells, and hydrogen production. It is worth noting that

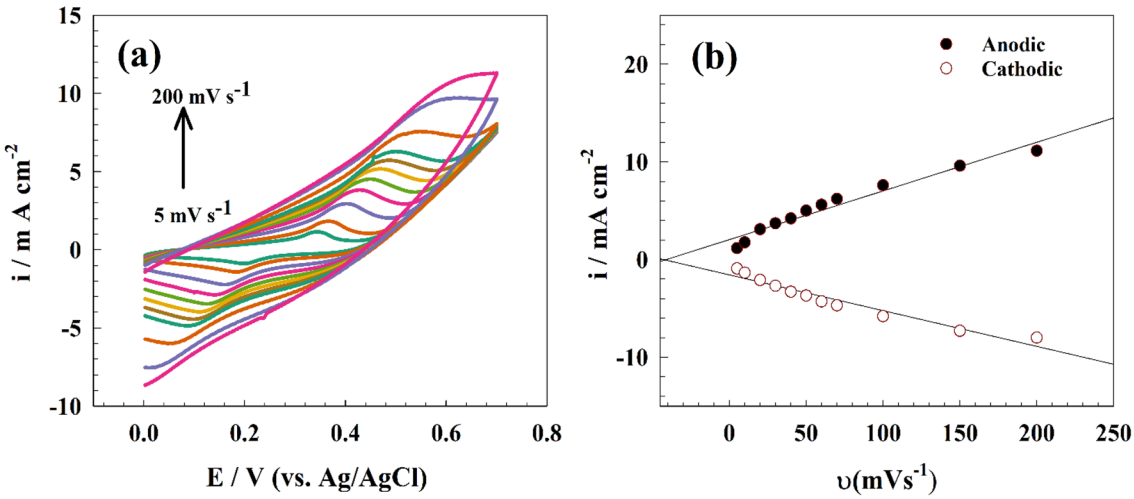

Figure 7. (**a**) CV of modified NMO-CF in 1.0 M NaOH at different scan rates, (**b**) linear relation between peak current versus of scan rate.

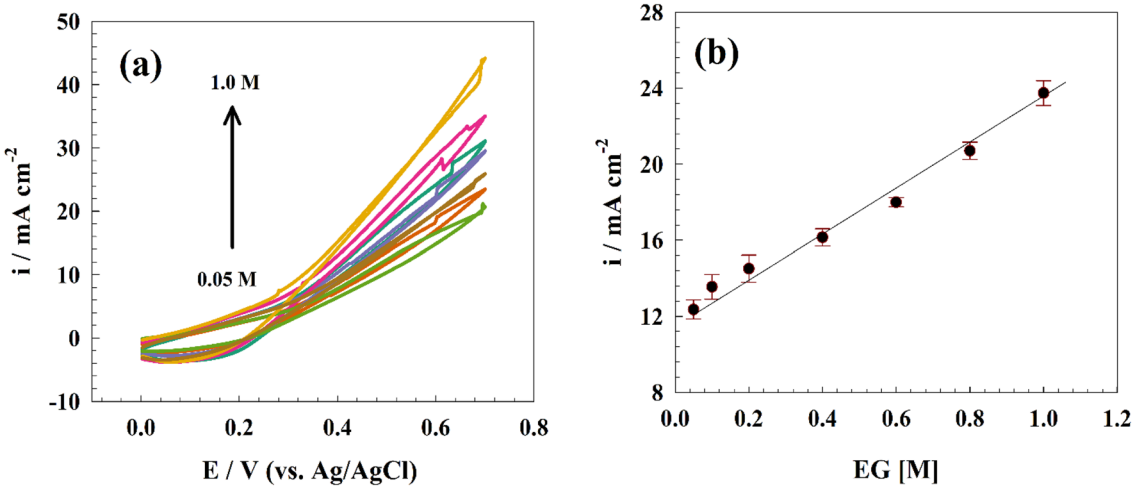

Figure 8. (**a**) CV of NMO-CF for different ethylene glycol concentrations, (**b**) linear relation between anodic current and ethylene glycol concentrations.

the effectiveness of this process is observed across a range of ethylene glycol concentrations. Figure 8b illustrates the correlation between the concentration of ethylene glycol and the magnitude of the anodic peak current.

For additional electrocatalyst experiments, cyclic voltammetry was used to examine the effects of various scan rate ranges of (5–200 mV s^{-1}) in the solution of 1.0 M ethylene glycol and 1.0 M NaOH, as shown in Fig. 9a.

The linear relationship created by graphing the anodic peaks current against the square root of scan rates is shown in Fig. 9b, The ethylene glycol oxidation process on the pre-prepared electrocatalysts is diffusion-controlled, and the diffusion coefficient was calculated using the following Randles–Sevcik equation based on the slope of the Ip vs. $\nu^{1/2}$ linear relation[59,60]:

$$I_p = 2.99 \times 10^5 n\,(1-\alpha) n_o A C_o D^{0.5} \upsilon^{0.5} \quad (7)$$

The maximum oxidation current is Ip, the anodic charge transfer coefficient is α, υ is the scan rate (V s^{-1}), C_o is the initial ethylene glycol concentration (mol cm^3), and D is the diffusion coefficient (mol cm^{-1}) and A the electrode's surface area. The diffusion coefficient estimated for modified NMO-CF as 1.6×10^{-7} mol cm^{-1}. However, the small diffusion coefficient value for ethylene glycol toward the NMO-CF electrode can be examined by high ethylene glycol viscosity that limits the movement of fuel molecules through the carbon felt electrode. The difficulties of ethylene glycol diffusion can also be observed by slight changes in the anodic current density with the increased scan rate, as indicated in Fig. 9a.

The endurance of NMO-CF and CF were assessed by observing the constant potential chronoamperometry over a period of 10 h, while maintaining a constant potential of 0.55 V (vs. Ag/AgCl) (see Fig. 10). In case of

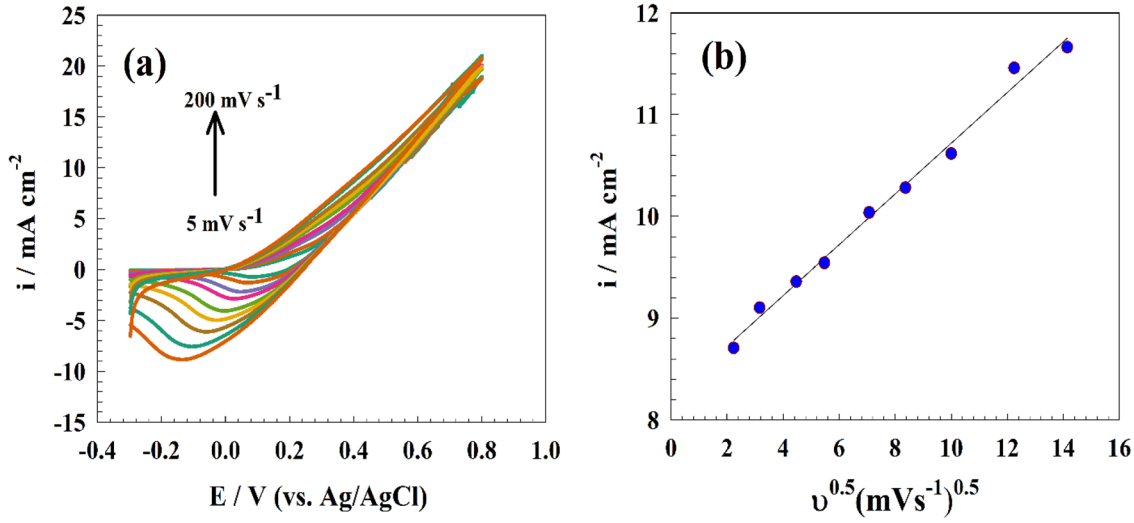

Figure 9. CVs of NMO-CF in ethylene glycol and NaOH at different scan rates, (**b**) Linear relation between anodic current versus square root of scan rate.

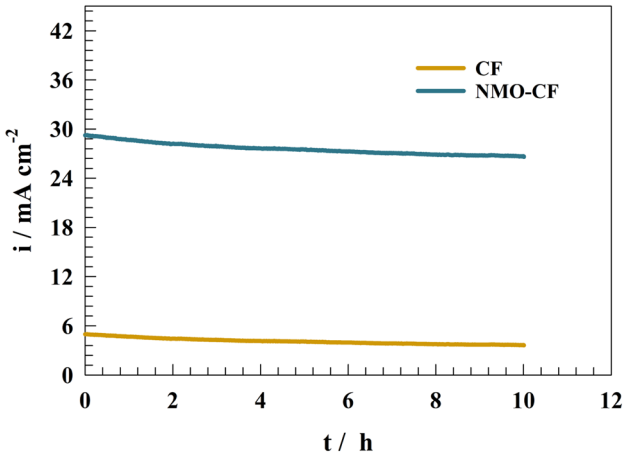

Figure 10. Long-term stability of ethylene glycol after 10 h of oxidation.

NMO-CF, a high stability can be noticed for ethylene glycol oxidation. Whereas, the current decreased by 9.8% of the initial value after 10 h of continuous oxidation. The decrement current can be explained by accumulation of residual carbon materials or formation of nickel/manganese carbonate after adsorption of CO as a result of oxidation process. Furthermore, mechanical corrosion of electrode by gas evolution after ethylene glycol conversion. Therefore, presence of NMO nanoparticles improved the stability of CF towards the ethylene glycol oxidation.

Hydrogen evolution

The second aim of this study was to examine the HER on a surface that has undergone modification using NMO-CF. Figure 11a illustrates the linear sweep voltammetry of the NMO-CF surface in alkaline medium. The merging of carbon support with spinel oxides led to a discernible enrichment in current density for the improved NMO-CF. The alteration resulted in enhancements in both the electrical and adsorption properties. The hydrogen evolution reaction (HER) can be mathematically described in an alkaline environment using the following steps: The Volmer step, also referred to as the first stage of HER, involves the adsorption of hydrogen ions onto the surface of the electrode. In the subsequent phase, also known as the Tafel reaction, two adsorbed hydrogen ions on the surface combine. Alternately, the phenomenon may involve the Heyrovsky mechanism, which involves the formation of a direct bond between a hydrated proton in the medium and a surface-adsorbed hydrogen atom.

The application of the Tafel polarization curve by using LSV facilitates the determination of the rate-controlling step, specifically either the first or subsequent step, in HER. The Tafel plot depicted in Fig. 11b showcases the performance of the NMO-CF electrode in the context of HER. The Tafel slopes of modified an unmodified carbon felt, revealing that NMO-CF exhibits a Tafel slope of 98 mV dec^{-1}, whereas untreated carbon felt has a Tafel slope of 138 mV dec^{-1}. The Tafel slope value for the NMO-CF was consistent with previous modified surface values published for the Ag@CNT/glassy carbon (148 mV dec^{-1})[61] and Ni_2Fe@porous carbon (83 mV dec^{-1})[62].

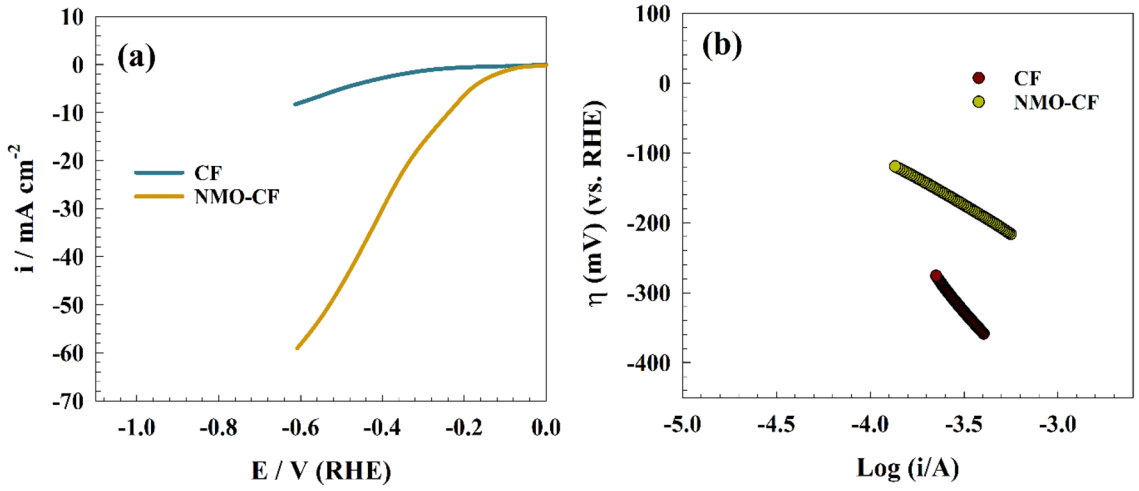

Figure 11. Linear sweep voltammetry of modified surfaces for HER., (**b**) Tafel plot of hydrogen evolution upon CF an NMO-CF electrodes.

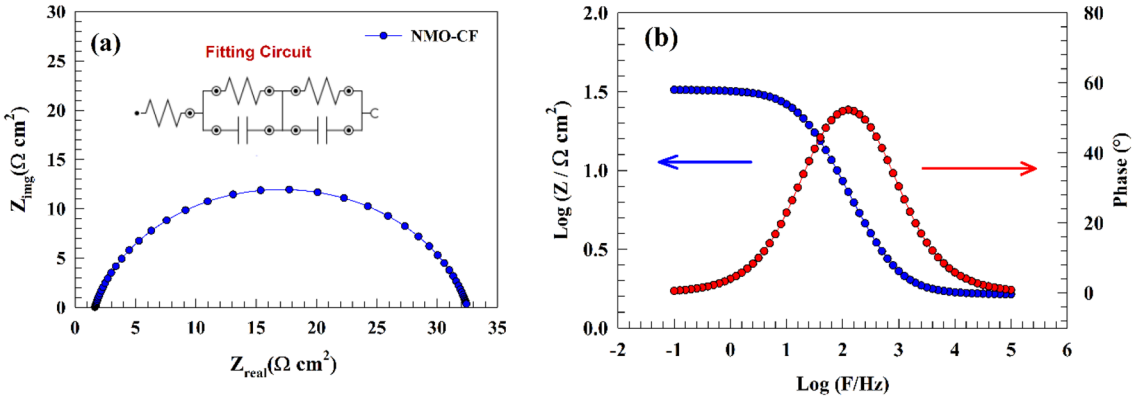

Figure 12. EIS representation of NMO-CF (**a**) Nyquist, (**b**) Bode plots.

Electrode	Rs (Ω cm^{-2})	R_1 (Ω cm^{-2})	C1 (F)	R_2 (Ω cm^{-2})	C2 (F)
NMO-CF	2.15	3.21	0.0000173	33.74	0.000308

Table 1. EIS parameters for NMO-CF electrode for HER.

The utilization of electrochemical impedance spectroscopy (EIS) was employed to examine the HER of the modified NMO-CF electrodes. Figure 12a demonstrates the use of HER through the utilization of electrochemical impedance spectroscopy (EIS) while subjecting it to a consistent alternating current (AC) potential of − 0.45 V relative to the reversible hydrogen electrode (RHE). The magnitudes of resistance exhibited variability; nevertheless, the Nyquist plot created by the modified electrode NMO-CF consistently revealed semi-circular patterns. The electrochemical manufacturing process can be described as a phenomenon involving the transfer of charges, as supported by the data acquired using electrochemical impedance spectroscopy (EIS). The EIS data was analyzed by employing the NOVA software for fitting purposes. The NMO-CF electrode demonstrated a dual circuit topology, where one cell was connected to the solution resistance. The capacitor and resistance were connected in parallel within the cell, as seen in the inset of Fig. 12a.

In addition, the presence of a constant phase component signifies the presence of surface heterogeneity, which has implications for the effectiveness of hydrogen production. The measured charge transfer resistance of the NMO-CF surface is determined to be 33 Ω cm^{-2}. A favorable link has been seen between a reduction in resistance value and an augmentation in electrode activity. The estimated parameters of the electrochemical impedance spectroscopy (EIS) results are presented in Table 1. The properties of the modified electrodes NMO-CF when exposed to a potential of − 0.45 V in a 1.0 M NaOH solution are depicted in Fig. 12b, which showcases the bode graphs. Whereas, the pure charge transfer process can be observed. The associated Bode plot shows how the nanostructured thin films act as electrocatalysts. According to the Bode figure, the phase angles at the highest frequency (f_{max}) exhibit the following conductive trend at phase angle 53°.

Conclusion

The nickel manganese loaded to carbon felt was successfully prepared using the hydrothermal method. Whereas the structure of the prepared materials was characterized using different analytical techniques.

The electrode showed high activity toward ethylene glycol oxidation and hydrogen production in an alkaline medium. The diffusion of ethylene glycol toward the NMO-CF electrode was observed to be slightly small due to the interaction between EG and water. Furthermore, the electrode showed noticeable stability after 10 h of continuous oxidation. Thus, the electrode's durability is verified by structure stability by scanning electron microscopy. On the other hand, the NMO-CF reached a high current density (50 mA cm^{-2}) for hydrogen production at an overpotential of 480 mV (vs. RHE).

Data availability

The datasets used and/or analysed during the current study are available from the corresponding author on reasonable request.

Received: 6 November 2023; Accepted: 28 December 2023
Published online: 04 January 2024

References

1. Lasia, A. Hydrogen evolution reaction. *Handb. Fuel Cells* **2**, 416–440 (2010).
2. Dubouis, N. & Grimaud, A. The hydrogen evolution reaction: from material to interfacial descriptors. *Chem. Sci.* **10**, 9165–9181 (2019).
3. Bashal, A. H. *et al.* Green synthesis of NiFe2O4 nano-spinel oxide-decorated carbon nanotubes for efficient capacitive performance, effect of electrolyte concentration. *Nanomaterials.* https://doi.org/10.3390/nano13192643 (2023).

4. Gamal, H., Elshahawy, A. M., Medany, S. S., Hefnawy, M. A. & Shalaby, M. S. Recent advances of vanadium oxides and their derivatives in supercapacitor applications: A comprehensive review. *J. Energy Storage* **76**, 109788. https://doi.org/10.1016/j.est.2023.109788 (2024).
5. Fashedemi, O. O. Microwave-assisted synthesis of palladium-based core-shell nanocatalysts and iron phthalocyanines and their applications in direct alkaline alcohol fuel cells (2013).
6. Kamarudin, M. Z. F., Kamarudin, S. K., Masdar, M. S. & Daud, W. R. W. Direct ethanol fuel cells. *Int. J. Hydrogen Energy.* **38**, 9438–9453 (2013).
7. An, L. & Chen, R. Recent progress in alkaline direct ethylene glycol fuel cells for sustainable energy production. *J. Power Sources.* **329**, 484–501. https://doi.org/10.1016/j.jpowsour.2016.08.105 (2016).
8. Xin, L., Zhang, Z., Qi, J., Chadderdon, D. & Li, W. Electrocatalytic oxidation of ethylene glycol (EG) on supported Pt and Au catalysts in alkaline media: Reaction pathway investigation in three-electrode cell and fuel cell reactors. *Appl. Catal. B Environ.* **125**, 85–94. https://doi.org/10.1016/j.apcatb.2012.05.024 (2012).
9. Miyazaki, K. *et al.* Electrochemical oxidation of ethylene glycol on Pt-based catalysts in alkaline solutions and quantitative analysis of intermediate products. *Electrochim. Acta.* **56**, 7610–7614. https://doi.org/10.1016/j.electacta.2011.06.078 (2011).
10. Christensen, P. A. & Hamnett, A. The oxidation of ethylene glycol at a platinum electrode in acid and base: An in situ FTIR study. *J. Electroanal. Chem. Interfacial Electrochem.* **260**, 347–359. https://doi.org/10.1016/0022-0728(89)87149-9 (1989).
11. Medany, S. S. & Hefnawy, M. A. Nickel–cobalt oxide decorated chitosan electrocatalyst for ethylene glycol oxidation. *Surf. Interfaces* https://doi.org/10.1016/j.surfin.2023.103077 (2023).
12. Nayak, S. P., Ventrapragada, L. K., Rao, A. M. & Kumar, J. K. K. Porous gold-curcumin nanocomposite for enhanced electrooxidation of glycerol and ethylene glycol. *Mater. Lett.* **330**, 133212 (2023).
13. Gupta, S., & De, M. Role of metal (Cu/Ni/Fe/Co)-carbon composite in enhancing electro-oxidation of ethylene glycol. *J. Appl. Electrochem*. 1–15 (2023).
14. Rajeswari, B. *et al.* Ethylene glycol-assisted synthesis of reduced graphene oxide-supported bimetallic Pt-Co nanoparticles for the ultra-sensitive detection of tert-butyl hydroquinone. *Inorg. Chem. Commun.* **151**, 110627 (2023).
15. Hai, B., Huang, W., & Li, J. Promotion effects of Pr-doped CeO2· H2O to Pt catalysts toward alcohol electrooxidation reaction. *Mater. Lett.* 134796 (2023).
16. Li, X. *et al.* Ag-doped Pd nano-dendritic for promoting the electrocatalytic oxidation of ethylene to ethylene glycol. *Mater. Chem. Front.* **7**, 1437–1445 (2023).
17. Hefnawy, M. A., Fadlallah, S. A., El-Sherif, R. M. & Medany, S. S. Nickel-manganese double hydroxide mixed with reduced graphene oxide electrocatalyst for efficient ethylene glycol electrooxidation and hydrogen evolution reaction. *Synth. Met.* **282**, 116959. https://doi.org/10.1016/j.synthmet.2021.116959 (2021).
18. Hefnawy, M. A., Medany, S. S., El-Sherif, R. M., El-Bagoury, N. & Fadlallah, S. A. High-performance IN738 superalloy derived from turbine blade waste for efficient ethanol, ethylene glycol, and urea electrooxidation. *J. Appl. Electrochem.* https://doi.org/10.1007/s10800-023-01862-7 (2023).
19. Hefnawy, M. A., Fadlallah, S. A., El-Sherif, R. M. & Medany, S. S. Systematic DFT studies of CO-Tolerance and CO oxidation on Cu-doped Ni surfaces. *J. Mol. Graph. Model.* **118**, 108343. https://doi.org/10.1016/j.jmgm.2022.108343 (2023).
20. Li, Z. *et al.* Tuning concave PtSn nanocubes for efficient ethylene glycol and glycerol electrocatalysis. *Int. J. Hydrogen Energy.* **43**, 22538–22547. https://doi.org/10.1016/j.ijhydene.2018.10.132 (2018).
21. Hefnawy, M. A., Fadlallah, S. A., El-Sherif, R. M. & Medany, S. S. Synergistic effect of Cu-doped NiO for enhancing urea electrooxidation: Comparative electrochemical and DFT studies. *J. Alloys Compd.* **896**, 162857. https://doi.org/10.1016/j.jallcom.2021.162857 (2022).
22. Alamro, F. S. *et al.* Chitosan supports boosting NiCo2O4 for catalyzed urea electrochemical removal application. *Polymers* https://doi.org/10.3390/polym15143058 (2023).
23. Eliwa, A. S. *et al.* Ultrasonic-assisted synthesis of nickel metal-organic framework for efficient urea removal and water splitting applications. *Synth. Met.* **294**, 117309. https://doi.org/10.1016/j.synthmet.2023.117309 (2023).
24. Eliwa, A. S. *et al.* Synthesis and characterization of lead-based metal–organic framework nano-needles for effective water splitting application. *Sci. Rep.* **13**, 12531. https://doi.org/10.1038/s41598-023-39697-z (2023).
25. Al-Kadhi, N. S. *et al.* Zinc nanocomposite supported chitosan for nitrite sensing and hydrogen evolution applications. *Polymers (Basel)* https://doi.org/10.3390/polym15102357 (2023).
26. Pierożyński, B. & Mikołajczyk, T. Hydrogen evolution reaction at Ru-modified nickel-coated carbon fibre in 0.1 M NaOH. *Polish J. Chem. Technol.* **17**, 18–22 (2015).
27. Koca, M. B., Çelik, G. G., Kardaş, G. & Yazıcı, B. NiGa modified carbon-felt cathode for hydrogen production. *Int. J. Hydrogen Energy.* **44**, 14157–14163 (2019).
28. Yue, X.-Y. *et al.* Wettable carbon felt framework for high loading Li-metal composite anode. *Nano Energy.* **60**, 257–266 (2019).
29. Yun, W. H. *et al.* Ni–Fe phosphide deposited carbon felt as free-standing bifunctional catalyst electrode for urea electrolysis. *Sci. Rep.* **11**, 22003 (2021).
30. Hefnawy, M. A., Fadlallah, S. A., El-Sherif, R. M. & Medany, S. S. Competition between enzymatic and non-enzymatic electrochemical determination of cholesterol. *J. Electroanal. Chem.* **930**, 117169. https://doi.org/10.1016/j.jelechem.2023.117169 (2023).
31. Şahin, E. A. Preparation of CoAg modified carbon felt electrodes for alkaline water electrolysis. *Russ. J. Phys. Chem. A.* **96**, 664–672 (2022).
32. Hu, J., Zhou, Y., Liu, Y., Xu, Z. & Li, H. Recent advances in manganese-based materials for electrolytic water splitting. *Int. J. Mol. Sci.* **24**, 6861 (2023).
33. Zhao, M., Zhang, S., Lin, J., Hu, W. & Li, C. M. Synergic effect of Fe-doping and Ni3S2/MnS heterointerface to boost efficient oxygen evolution reaction. *Electrochim. Acta.* **430**, 141088 (2022).
34. Zhu, J. *et al.* Study of active sites on Se-MnS/NiS heterojunctions as highly efficient bifunctional electrocatalysts for overall water splitting. *J. Mater. Chem. A.* **7**, 26975–26983 (2019).
35. Zhong, D., Liu, Y., Liao, X., Zhong, N. & Xu, Y. Facile preparation of binder-free NiO/MnO2-carbon felt anode to enhance electricity generation and dye wastewater degradation performances of microbial fuel cell. *Int. J. Hydrogen Energy.* **43**, 23014–23026 (2018).
36. Achour, W. *et al.* Hydrothermal deposition of urchin-like NiCo2O4 on carbon felt as performed flexible electrodes for supercapacitors. *J. Appl. Electrochem.* **53**, 1405–1419. https://doi.org/10.1007/s10800-023-01863-6 (2023).
37. Menezes, P. W. *et al.* Using nickel manganese oxide catalysts for efficient water oxidation. *Chem. Commun.* **51**, 5005–5008. https://doi.org/10.1039/C4CC09671A (2015).
38. Park, T.-Y., MuraleeGopi, C. V. V., Ahn, J.-W. & Kim, H.-J. Facile preparation of nanoflake MnNi2O4–PbS nanoparticle composites on Ni foam as advanced electrode materials for supercapacitors. *New J. Chem.* **42**, 14157–14162. https://doi.org/10.1039/C8NJ02709A (2018).
39. Rekhila, G., Gabes, Y., Bessekhouad, Y. & Trari, M. Hydrogen production under visible illumination on the spinel NiMn2O4 prepared by sol gel. *Sol. Energy.* **166**, 220–225. https://doi.org/10.1016/j.solener.2018.02.064 (2018).
40. Periyasamy, S. *et al.* Exceptionally active and stable spinel nickel manganese oxide electrocatalysts for urea oxidation reaction. *ACS Appl. Mater. Interfaces.* **8**, 12176–12185. https://doi.org/10.1021/acsami.6b02491 (2016).

41. Ding, J. *et al.* Enhanced photocatalytic reduction for the dechlorination of 2-chlorodibenzo-p-dioxin by high-performance g-C3N4/NiO heterojunction composites under ultraviolet-visible light illumination. *J. Hazard. Mater.* **384**, 121255. https://doi.org/10.1016/j.jhazmat.2019.121255 (2020).
42. Chaudhary, S., Kaur, Y., Jayee, B., Chaudhary, G. R. & Umar, A. NiO nanodisks: Highly efficient visible-light driven photocatalyst, potential scaffold for seed germination of Vigna Radiata and antibacterial properties. *J. Clean. Prod.* **190**, 563–576. https://doi.org/10.1016/j.jclepro.2018.04.110 (2018).
43. Zhou, Q. *et al.* Fabrication and characterization of highly sensitive and selective sensors based on porous NiO nanodisks. *Sens. Actuators B Chem.* **259**, 604–615. https://doi.org/10.1016/j.snb.2017.12.050 (2018).
44. Tong, S. *et al.* Mesoporous NiO with a single-crystalline structure utilized as a noble metal-free catalyst for non-aqueous Li–O2 batteries. *J. Mater. Chem. A.* **3**, 16177–16182. https://doi.org/10.1039/C5TA03685B (2015).
45. Zhang, Y. *et al.* Ag2O loaded NiO ball-flowers for high performance supercapacitors. *Mater. Lett.* **177**, 71–75. https://doi.org/10.1016/j.matlet.2016.04.169 (2016).
46. Lee, J. W., Ahn, T., Soundararajan, D., Ko, J. M. & Kim, J.-D. Non-aqueous approach to the preparation of reduced graphene oxide/α-Ni (OH) 2 hybrid composites and their high capacitance behavior. *Chem. Commun.* **47**, 6305–6307 (2011).
47. Ma, J., Yin, L. & Ge, T. 3D hierarchically mesoporous Cu-doped NiO nanostructures as high-performance anode materials for lithium ion batteries. *CrystEngComm.* **17**, 9336–9347. https://doi.org/10.1039/C5CE00818B (2015).
48. Cao, L., Wang, D. & Wang, R. NiO thin films grown directly on Cu foils by pulsed laser deposition as anode materials for lithium ion batteries. *Mater. Lett.* **132**, 357–360 (2014).
49. Ren, Y. *et al.* Fabrication of NiO nanowires/G composite as electrode material for high performance supercapacitor. *Int. J. Electrochem. Sci.* **9**, 7206–7216 (2014).
50. Islam, M. B., Yanagida, M., Shirai, Y., Nabetani, Y. & Miyano, K. NiO x hole transport layer for perovskite solar cells with improved stability and reproducibility. *ACS Omega.* **2**, 2291–2299 (2017).
51. Tian, Y. *et al.* Novel binder-free electrode of NiCo2O4@ NiMn2O4 core-shell arrays modified carbon fabric for enhanced electrochemical properties. *Ceram. Int.* **45**, 16904–16910 (2019).
52. Wang, Z., Zhu, Z., Zhang, C., Xu, C. & Chen, C. Facile synthesis of reduced graphene oxide/NiMn2O4 nanorods hybrid materials for high-performance supercapacitors. *Electrochim. Acta.* **230**, 438–444. https://doi.org/10.1016/j.electacta.2017.02.023 (2017).
53. Rohokale, M. S., Dhabliya, D., Sathish, T., Vijayan, V. & Senthilkumar, N. A novel two-step co-precipitation approach of CuS/NiMn2O4 heterostructured nanocatalyst for enhanced visible light driven photocatalytic activity via efficient photo-induced charge separation properties. *Phys. B Condens. Matter.* **610**, 412902 (2021).
54. Busacca, C. *et al.* Electrospun NiMn2O4 and NiCo2O4 spinel oxides supported on carbon nanofibers as electrocatalysts for the oxygen evolution reaction in an anion exchange membrane-based electrolysis cell. *Int. J. Hydrogen Energy.* **44**, 20987–20996 (2019).
55. Saha, S. *et al.* Effect of particle morphology on the electrochemical performance of hydrothermally synthesized NiMn2O4. *Electrochim. Acta.* **353**, 136515 (2020).
56. Al-Kadhi, N. S. *et al.* Polyaniline-supported nickel oxide flower for efficient nitrite electrochemical detection in water. *Polymers (Basel).* https://doi.org/10.3390/polym15071804 (2023).
57. Hefnawy, M. A., Medany, S. S., El-Sherif, R. M. & Fadlallah, S. A. NiO-MnOx/polyaniline/graphite electrodes for urea electrocatalysis: Synergetic effect between polymorphs of MnOx and NiO. *ChemistrySelect* **7**, e202103735. https://doi.org/10.1002/slct.202103735 (2022).
58. Lin, Q., Wei, Y., Liu, W., Yu, Y. & Hu, J. Electrocatalytic oxidation of ethylene glycol and glycerol on nickel ion implanted-modified indium tin oxide electrode. *Int. J. Hydrogen Energy.* **42**, 1403–1411. https://doi.org/10.1016/j.ijhydene.2016.10.011 (2017).
59. Hefnawy, M. A., Medany, S. S., El-Sherif, R. M. & Fadlallah, S. A. Green synthesis of NiO/Fe3O4@chitosan composite catalyst based on graphite for urea electro-oxidation. *Mater. Chem. Phys.* **290**, 126603. https://doi.org/10.1016/j.matchemphys.2022.126603 (2022).
60. Hefnawy, M. A., Medany, S. S., Fadlallah, S. A., El-Sherif, R. M. & Hassan, S. S. Novel self-assembly Pd(II)-schiff base complex modified glassy carbon electrode for electrochemical detection of paracetamol. *Electrocatalysis.* https://doi.org/10.1007/s12678-022-00741-7 (2022).
61. Hefnawy, M. A., Nafady, A., Mohamed, S. K. & Medany, S. S. Facile green synthesis of Ag/carbon nanotubes composite for efficient water splitting applications. *Synth. Met.* **294**, 117310. https://doi.org/10.1016/j.synthmet.2023.117310 (2023).
62. Chang, J. *et al.* Nitrogen-doped porous carbon encapsulated nickel iron alloy nanoparticles, one-step conversion synthesis for application as bifunctional catalyst for water electrolysis. *Electrochim. Acta.* **389**, 138785. https://doi.org/10.1016/j.electacta.2021.138785 (2021).

Author contributions

S.S.M.: Formal analysis, Funding acquisition, Methodology, Data curation, Conceptualization, Validation, Project administration, Resources, Software, Writing—original draft, Writing—review & editing. M.A.H.: Formal analysis, Funding acquisition, Methodology, Data curation, Conceptualization, Validation, Project administration, Resources, Software, Writing—original draft, Writing—review & editing. S.M.K.: Formal analysis, Funding acquisition, Methodology, Data curation, Conceptualization, Validation, Project administration, Resources, Software, Writing—original draft Writing—review & editing.

Funding

Open access funding provided by The Science, Technology & Innovation Funding Authority (STDF) in cooperation with The Egyptian Knowledge Bank (EKB).

Competing interests

The authors declare no competing interests.

Additional information

Correspondence and requests for materials should be addressed to S.S.M. or M.A.H.

Reprints and permissions information is available at www.nature.com/reprints.

Publisher's note Springer Nature remains neutral with regard to jurisdictional claims in published maps and institutional affiliations.